Contact resistance study of high-copper alloys used in power automotive connectors

R El Abdi[1]*, **A Beloufa**[2], and **N Benjemaâ**[2]
[1]Larmaur – Rennes1 University, Rennes, France
[2]IPR – Rennes1 University, Palms, Rennes, France

The manuscript was received on 23 December 2007 and was accepted after revision for publication on 26 March 2008.

DOI: 10.1243/09544070JAUTO799

Abstract: Contact resistance of the copper alloys used in automotive connectors was studied in the literature, but no study has been undertaken in order to optimize this resistance for the new high-copper alloys intended for power automotive connectors.

This study was carried out in order to determine the changes in resistance for different loadings and contact geometries. A new generation of high-performance copper alloys was analysed. The used samples were U shaped with a segment containing a sphere and were subjected to insertion (sliding contact) and indentation (static contact) tests. A finite element simulation using the ANSYS code gave contact modellings with or without roughness; this roughness was measured with a profilometer. Numerical modelling of the contact surfaces when the roughness of the materials was taken into account led to results close to the experimental results especially in the case of the lower forces during the indentation test. On the other hand, a relation between the contact resistance and the contact force was established.

These results could help in the choice of a material to provide a good compromise concerning both the electrical and the mechanical aspects for a power connector used for automotive industry.

Keywords: contact resistance, high-copper alloys, finite element modelling, roughness, power automotive connectors

1 INTRODUCTION

Studies of connectors for electric and electronic systems have been and still are being pursued. The electrical connector reliability is mainly linked to the mechanical behaviour of the contact zone. The electrical resistance of the connector is related to this zone which is imposed by the connector design. Much work [**1**–**3**] has been devoted to understanding the contact zone mechanisms but their complexity led the present authors to study a simple contact form with earlier copper alloys.

In this study, a simple geometry (plane and spherical forms) represented elementary contact connectors. Pure copper is the optimal material for electric current conductors, but many wire and cable applications require a strength that exceeds the strength attainable with pure copper wire, e.g. connector pins. In these cases, the use of the high-copper alloys becomes necessary [**4**]. Several connectors made of new high-copper alloys were studied. The contact zones were subjected to normal loads to simulate an indentation test and to coupled normal and transverse loads to simulate an insertion test. Different copper alloy substrates were tested with different contact surface roughness profiles. A finite element modelling using the ANSYS code [**5**], taking into account the mechanical and the electrical phenomena, showed the influence of the roughness profile, of the mechanical and electrical copper alloy properties, and of the used sample sizes on the contact resistance.

The goal of this study was to minimize the contact resistance by an appropriate choice of copper alloys and contact geometries with a realistic contact force. A power law between contact resistance R_c and

**Corresponding author: IUT de Rennes - Départ. GMP, Rennes1 University, 3, Rue du Clos Courel, B. P. 90422, Rennes, 35704, France. email: relabdi@univ-rennes1.fr*

contact force F_c was established. This law will help connector manufacturers to design power connectors.

2 EXPERIMENTAL SET-UP AND SAMPLES USED

The present study analysed the contact resistance evolution for various high-copper alloy samples (including pure copper) submitted to different forces and with different sizes of the contact zone. The samples were produced with a sheet of 20 mm width, using the processing technique of stamping and bending.

The instrumented device consisted in applying indentation and insertion forces on two U-shaped samples (Fig. 1). One of the two samples was flat and the other contained a sphere with a radius R (Fig. 1). The two samples were fixed on the Teflon part 11 (Fig. 2). The contact force was imposed with the help of the vertical displacement of the micrometric table 9 which was activated by a step-by-step engine. This force was measured by a sensor 2. Another table 4 in translation movement was used to move the sample fixed on a translation turntable 12 horizontally via the connection parts 3. After the vertical contact force application, a horizontal displacement was produced. The insertion force was measured by the sensor 1 fixed on the micrometric table 4 which was actuated by a step-by-step engine (Fig. 2).

The experimental measurement bench was managed by a microcomputer over a general-purpose interface bus. This made it possible to produce an indentation phase (test 1) and an insertion phase under controlled forces (test 2).

1. The first test consisted in measuring the contact resistance by applying a progressive contact force F_c from 1 N to 100 N. The applied current was equal to 10 A (test known as the indentation test (Fig. 3(a))).
2. The second test consisted in applying a normal force and then a sliding of 1 mm to simulate the insertion in the connector. Forces F_c of 2 N, 4 N, 8 N, 16 N, 32 N, 64, and 100 Nwere used successively; the contact resistance was measured at the end of each insertion phase (Fig. 3(b)).

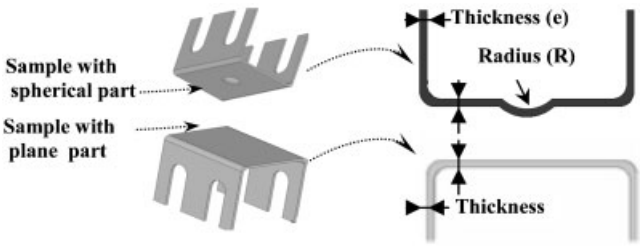

Fig. 1 U-shaped samples

Two voltmeters were connected to the packer sensors and these gave the insertion and the contact forces (measurements between 1 N and 130 N) and transmitted the measured values to the computer. A d.c. generator (Xantrax) was installed in order to transmit an electrical current to the two samples in contact. Another microvoltmeter (Keithley) with 1 μV resolution was used to measure the fall of potential by the 'four-wire' method. Thus, the contact resistance during insertion or at the end of the insertion phase could be obtained.

The two parts of the sample (plane part or lower part and a sphere segment or upper part) had the same thickness, i.e. 0.8 mm. The radius of the sphere segment was 2 mm or 3 mm (Fig. 1). The mechanical and electrical characteristics of the sample copper alloys are summarized in Table 1. These alloys were mass produced by Weiland-Werke AG Company [**4**]. Figure 4 shows the different behaviour laws (stress versus strain) for different copper alloys [**4**] that will be used to investigate the tested U-shaped samples.

Before each experiment, the sample surface was wiped with an antioxidant paste and then the sample was cleaned in an ultrasonic alcohol bath.

3 ELECTRICAL RESISTANCE

Measurements of the contact resistance for different contact forces for all copper alloys (for two sphere radii R of 2 mm and 3 mm and for an 0.8 mm sample thickness) were undertaken for indentation and insertion tests.

This experiment consisted in applying different contact forces (from 1 N to 100 N) and measuring the contact resistance when two spherical radii were considered. The current used was 10 A and the maximum voltage was equal to 1 V. The micrometric table moved vertically with a velocity of 1 mm/s with the help of a step-by-step engine with a precision of 1 μm.

3.1 Finite element models

In order to obtain a numerical simulation of different copper alloy behaviours and because of the axisymmetrical form of the sample spherical part (upper part, Fig. 1), only half of the samples were meshed (Fig. 5). Two finite element models are proposed with or without the contact surface roughness.

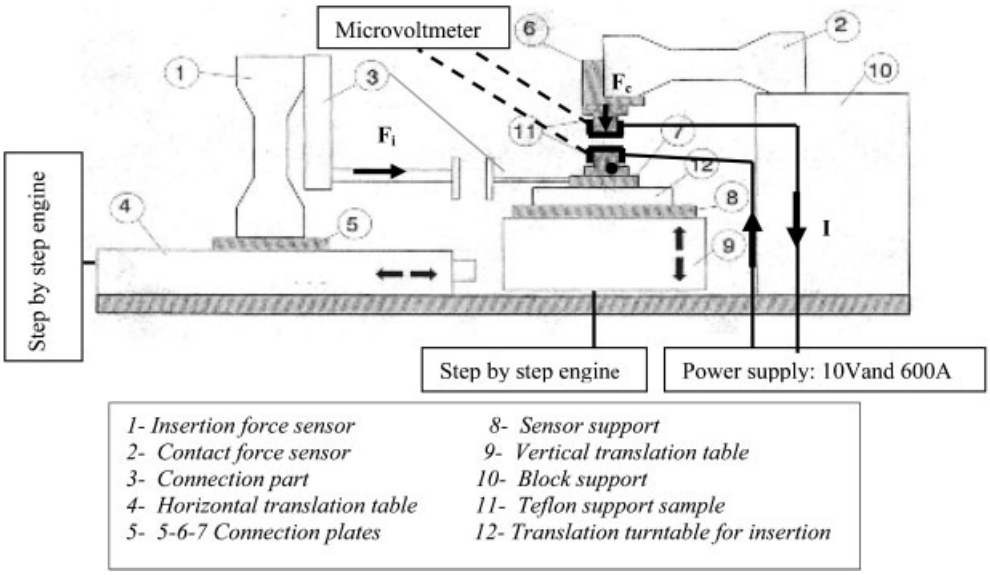

Fig. 2 Experimental set-up

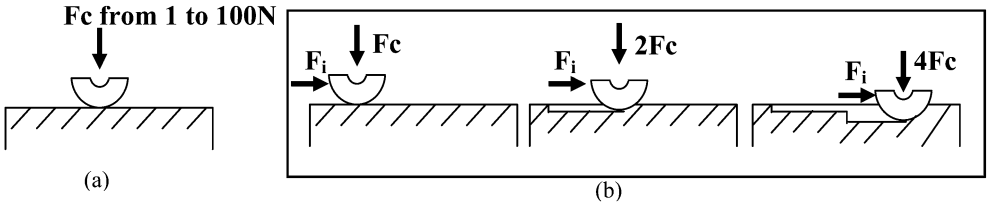

Fig. 3 Sample under (a) the indentation test and (b) the insertion test (spherical–plane contact)

The measurement of the roughness profile was obtained with the help of a profilometer. Figures 5(a) and 5(b) give the adopted meshes for these two configurations.

Simulation of the displacement for an axisymmetrical model and the large deformations with elastoplastic behaviour was obtained with the ANSYS finite element [**5**] code. Underlying the approach in this code is the discretization of the continuum involved. Also, an important feature of this program involved the ability to model the contact between the spherical part and the plane part as a sliding interface. Little by little, as the spherical part progressed during the indentation test, the program automatically established the junction between the contact surface nodes of the spherical surface and those of the plane. For the mechanical calculus, axisymmetrical element types were used: the axisymmetrical structural solid node element (Plane183) and three node surface-to-surface elements for the contact area (Conta172) and target area (Targe169). For the electrical calculus, plane eight-node coupled-field solid elements were used (Plane223-2D). These surface-to-surface contact elements used Gauss integration points as a contact detection point. The program checked the convergence of the iterative solution by using a force criterion. The friction coefficient μ between the two surfaces in

Table 1 Mechanical and electrical characteristics for the different copper alloys used [**4**]

Copper alloy	Composition	Yield stress (MPa)	Young's modulus (MPa)	Strain-hardening exponent	Tensile strength (MPa)	Vickers hardness (HV)	Thermal conductivity (W/mK)	Electrical resistivity (Ωmm) (IACS %)
Cub1	99.9% Cu + 0.008% P	200	1.2×10^5	0.18	240–300	65–95	340	2.12×10^{-5} (80%)
K09	99.99 Cu	200	1.2×10^5	0.18	240–300	65–95	401	1.678×10^{-5} (100%)
K55	Cu3–Ni–Si–Mg	514	1.22×10^5	0.0746	620–760	180–220	190	4×10^{-5} (43.1%)
K65	Cu–Fe–2P	401	0.89×10^5	0.0380	470–530	140–160	280	2.7×10^{-5} (63.8%)
K75	Cu–Cr–Si–Ti	420	1.18×10^5	0.0247	460–540	140–170	310	2.2×10^{-5} (77.6%)
K80	Cu–Fe–P	322	0.9×10^5	0.0257	360–440	100–130	350	1.88×10^{-5} (91.4%)
K81	Cu–0.15Sn	333.5	1.1×10^5	0.0158	420–490	120–140	350	1.96×10^{-5} (79.3%)

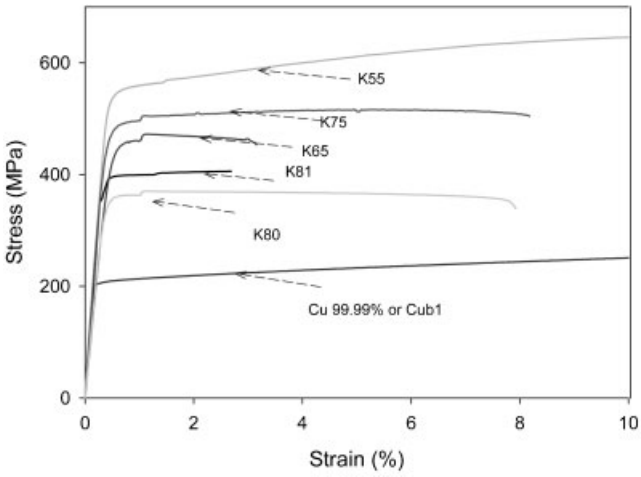

Fig. 4 Elastoplastic behaviour laws for different copper alloys

contact (copper alloy–copper alloy) was equal to 0.2. It is essential to note that, in this study, the indirect coupling solution was used. The software package is limited to 32 000 nodes because of cost. The program was used with 9817 elements and 28 313 nodes for the axisymmetrical model with the roughness modelization. A total of at least 708 elements was allowed to come into contact with the plane part in order to provide sufficient resolution in the computation of the field around the spherical part. Other smoothness meshes were tested. The conclusion was that the results were identical. To obtain better results, the contact zone was refined (Fig. 5, zoom of the contact zone). Owing to the axisymmetrical configuration, the boundary conditions may be expressed as

$$U_y(y=-0.8)=0 \tag{1}$$

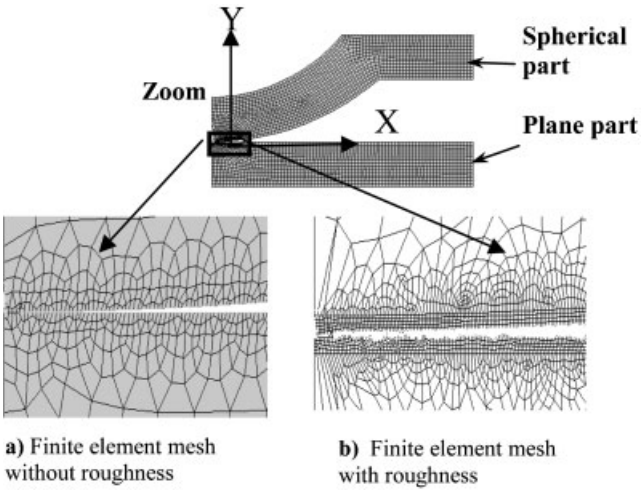

Fig. 5 Finite element meshes

where $y=-0.8$ mm denotes the lower surface of the plane part

$$U_x(x=0)=0 \tag{2}$$

where $x=0$ denotes the axisymetrical conditions. U_y and U_x are the displacements along the y and x axes respectively (Fig. 5).

3.2 Experimental results

Figure 6 shows that the contact resistance R_c can be fitted to a power law for all copper alloys according to

$$R_c=K_cF_c^{-n} \tag{3}$$

where F_c is the contact force and K_c depends on material properties and shapes and is given by

$$K_c=C\rho E^{1/3} \tag{4}$$

where C is a constant and ρ is the material resistivity [**6–8**]. However, the power n is close to 0.32–0.44 (Table 2 and Table 3).

The contact resistance presented a decrease versus the contact force (Fig. 6) for the segment sphere radius equal to 3 mm. K55 copper alloy presented a low conductivity, high hardness, and high Young's modulus (Table 1). This causes the highest contact resistance to be obtained (Fig. 6).

The same conclusions are obtained for other segment sphere radii, e.g. for the segment sphere radius equal to 2 mm (Fig. 7).

The contact resistance in both cases (insertion and indentation tests) was higher for the 2 mm sphere radius and conversely it was low for the largest sphere radius, 3 mm, for whichever contact force (Figs 6(a) and 7(a) or Figs 6(b) and 7(b)). Moreover, in the case of the insertion test, this resistance was lower than that obtained in the case of the indentation test (Figs 6(a) and (b) or Figs 7(a) and (b)), the contact surfaces becoming smoother after the insertion phase.

Figure 8 shows different imprints of the spherical and plane parts of sample. During the insertion phase, the vertical applied load increased from 1 N to 100 N. Then, the imprint broadened and became deeper (Fig. 8(b)); some remains were pulled out from the substrate. For the indentation test, the imprint has a circular form (Fig. 8(c)). The penetration depth of the sphere segment is equal to 3.1 μm (under a force of 100 N). Different scratches on the material surface were created during the copper

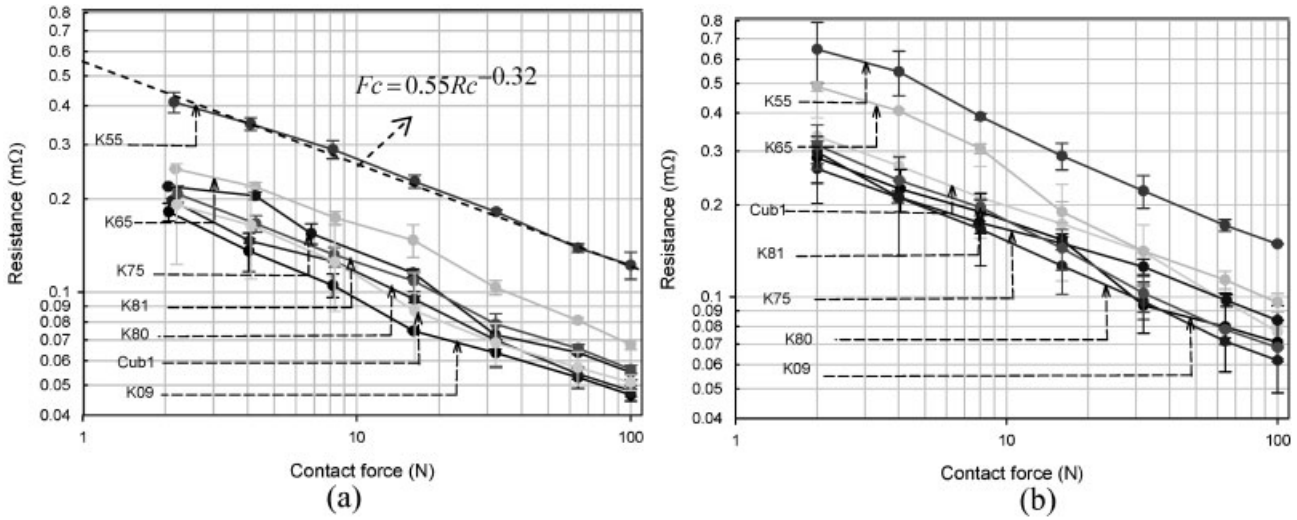

Fig. 6 Experimental resistances for different copper alloys ($R = 3$ mm and $e = 0.8$ mm) (a) sample under the insertion test; (b) sample under the indentation test

alloy manufacture and have an average depth of 2 μm and a width of 3 μm. The scratches were included in the roughness profile.

3.3 Numerical results

3.3.1 Indentation test

The experimental contact resistance data in the indentation test were rather higher than the numerical data (Fig. 9). Some attempts were made to improve the fit at lower forces by taking into account the roughness in the models. This seemed to improve the fit. Unfortunately, for higher forces the discrepancy remained between experimental and numerical data. To improve the convergence of the numerical model to the experimental model, some other factors should be examined (the contact spot caused by the wear of material, oxidation layers, etc.).

On the other hand during the experimental tests, the parallelism between the two plans of the two sample parts in contact as well as the surface roughness had a non-negligible influence on the resistance value determination.

For forces less than 10 N, the numerical results obtained when the modelling of the contact surface roughness was taken into account led to higher values than those obtained for a perfectly smooth contact zone (no roughness) and joined the experimental resistance values. However, when the vertical applied load was rather large (higher than 16 N), crushing of the asperities was obtained and the numerical modellings (with or without taking roughness into account) led to similar results (Fig. 9) (under a contact force of 16 N, the applied pressure in the plane surface is equal to 420 N/mm^2). The contact resistance took into account the resistance of constriction resistance and the contact asperity resistance. Thus, in the case of a numerical simulation where the contact surface was considered as a perfectly smooth zone, only the constriction resistance was taken into account. For the high forces, the numerical model is far away from the experimental values, because the numerical model by taking into account the roughness is considered as an axisymmetric model contrary to the real profile. Therefore, the numerical contact surface obtained at 100 N was not the same as the real

Table 2 Constant values of the resistance law for the insertion test ($R = 3$ mm)

Material	IACS (%)	K_c	n
K55	43.1	0.55	0.32
K65	63.8	0.33	0.35
K75	77.6	0.32	0.39
Cub1	80	0.25	0.35
K81	87.9	0.27	0.34
K80	91.4	0.25	0.36
K09	100	0.22	0.34

Table 3 Constant values of the resistance law for the indentation test ($R = 3$ mm)

Material	IACS (%)	K_c	n
K55	43.1	0.86	0.38
K65	63.8	0.69	0.44
K75	77.6	0.34	0.30
Cub1	80	0.44	0.36
K81	87.9	0.42	0.39
K80	91.4	0.34	0.37
K09	100	0.38	0.37

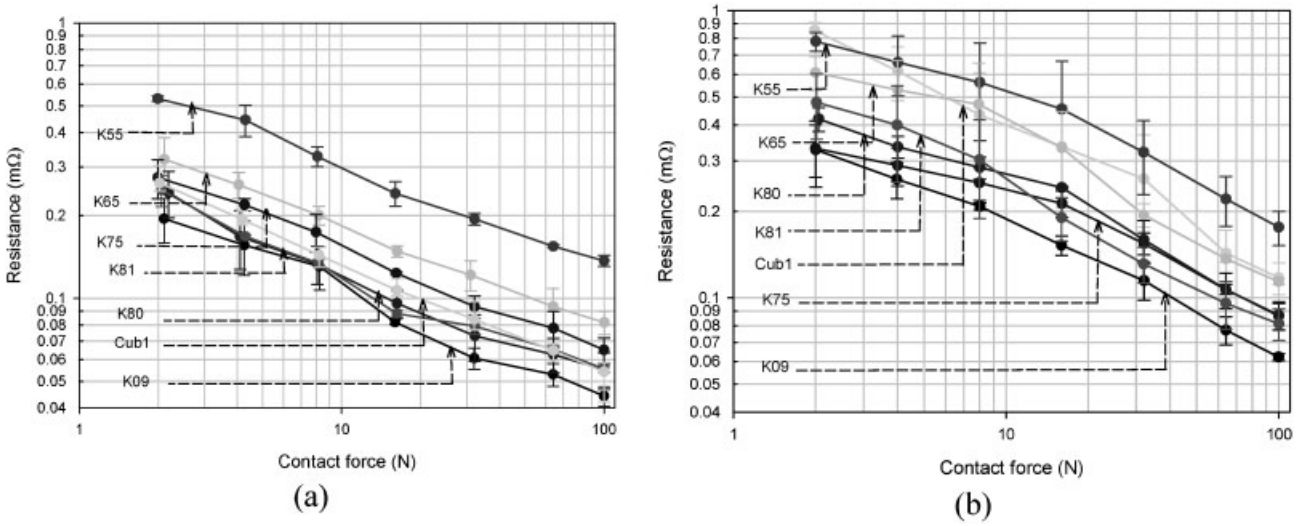

Fig. 7 Experimental resistances for different copper alloys ($R = 2$ mm and $e = 0.8$ mm) (a) sample under the insertion test; (b) sample under the indentation test

experimental contact surface (Figs 10(a) and (b)). However, if the real profile obtained at 100 N was introduced in the numerical modelling and the two contact surfaces were touching, the numerical resistance value approaches the experimental value (Figs 9(a) and (b), stars).

The numerical modelling taking into account the roughness profile led to a large number of elements, which results in a long calculation time. The axi-symmetric model is thus adequate for taking into account the roughness profile during the numerical simulation but it imposes a circular roughness profile. That is not really exact. Nevertheless, this approximation makes it possible to avoid a three-dimensional modelling, which will lead to exceeding the capacity permitted by the ANSYS university licence used.

Prior to the test, the roughness profile was obtained with a laser profiler (Taicaan). In general, the roughness profile was characterized by two parameters:

(a) the parameter P_a which relates to the average roughness deviation (Fig. 11) and is given by

$$P_a = \frac{1}{L}\int_0^L |Z(x)|\,\mathrm{d}x \tag{5}$$

(b) the parameter P_q which relates to the standard roughness deviation and is given by

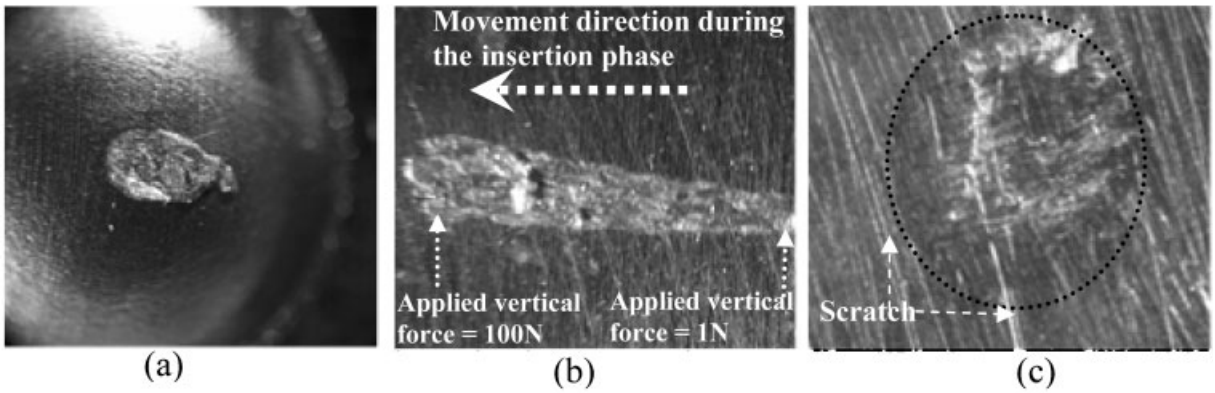

Fig. 8 (a) Imprint of the spherical part after the insertion phase (vertical applied force at the end of the insertion, 100 N) (K09 copper alloy; $R = 3$ mm); (b) imprint on the plane part after the insertion phase (K09 copper alloy; $R = 3$ mm); (c) imprint after the indentation test (vertical applied force, 100 N) (K09 copper alloy; $R = 3$ mm)

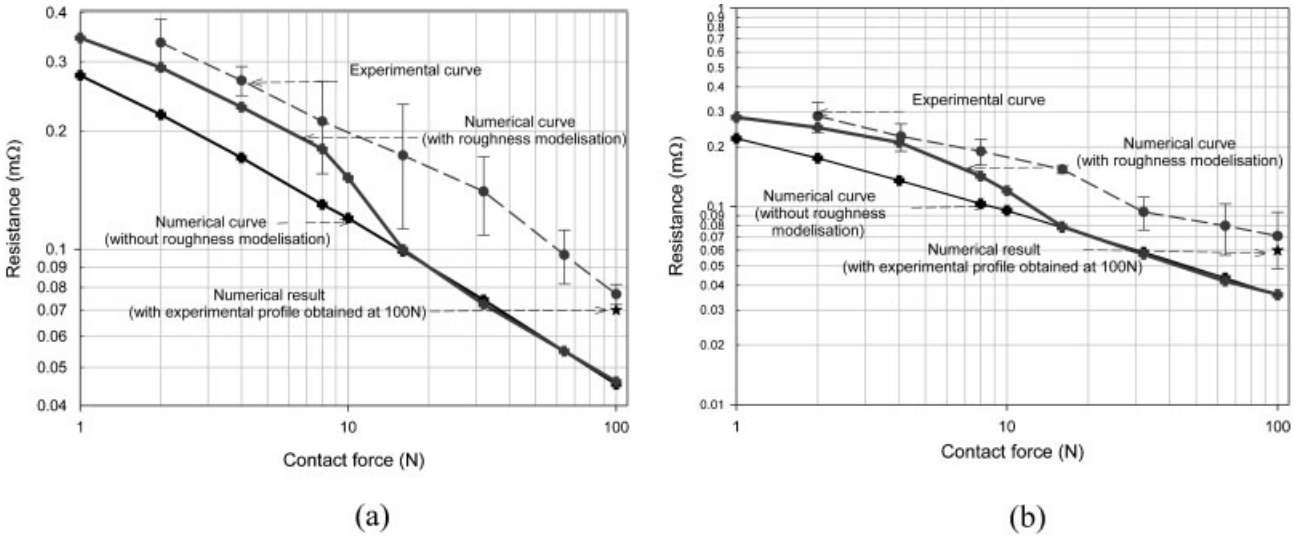

Fig. 9 Contact resistances for the indentation test for (a) Cub1 copper alloy and (b) K09 copper alloy ($R = 3$ mm and $e = 0.8$ mm)

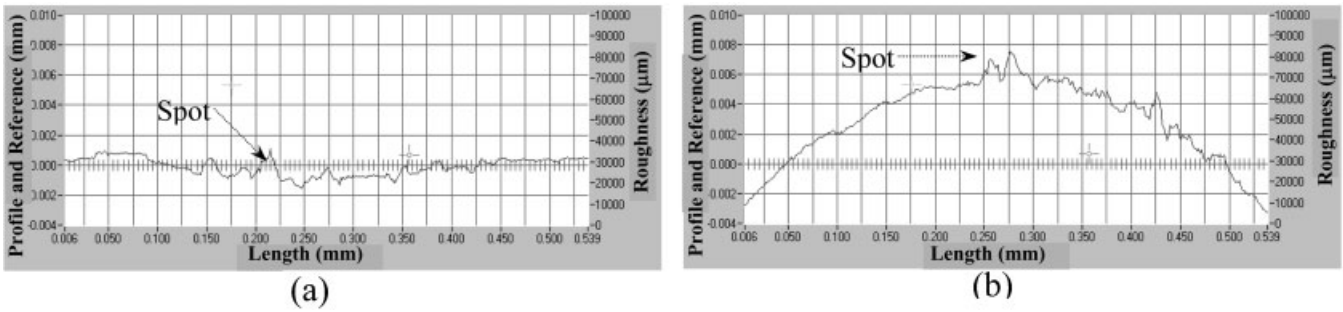

Fig. 10 Profiles of (a) the plane part and (b) the spherical part after an applied force of 100 N (K09 copper alloy; $R = 2$ mm)

$$P_q = \sqrt{\frac{1}{L}\int_0^L Z(x)^2 \, dx} \tag{6}$$

For the indentation test, Fig. 12 shows that, when the contact force is high ($F_c = 100$ N) the experimental contact resistance R_c becomes insensitive to the contact surface roughness since, under such a loading, the asperities are almost crushed.

Conversely, for relatively low contact forces (e.g. for 10 N) the roughness profile influenced the contact resistance as soon as the asperity amplitude became notable (Figs 9 and 12).

Figure 10 gives the worn profile surfaces of the contact zone after an applied indentation force of 100 N. The contact diameter obtained with the profilometer was equal to 0.34 mm (0.1 mm $\leqslant$ length $\leqslant$ 0.44 mm, see Fig. 10(a)) in the case of a segment of sphere with a 4 mm diameter.

For the high force value, the contact between the plane part and the segment sphere part was only located in the spot zone caused by the wear. The wear caused a high experimental contact resistance to be obtained in comparison with the numerical values [**9**, **10**] (Figs 9 and 12).

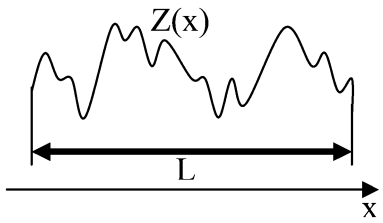

Fig. 11 Typical roughness profile

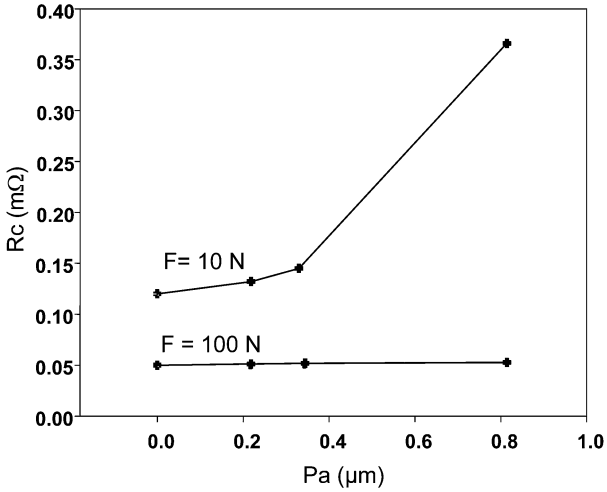

Fig. 12 Numerical electrical resistance versus the average deviation of the roughness for different indentation forces ($R = 2$ mm; Cub1 copper alloy) (indentation test)

3.3.2 Insertion test

For the insertion test (Fig. 3(b)), the numerical contact resistance (numerical model without roughness) was lower than the experimental values (Fig. 13); this could be due to the presence of remains and spots obtained under the wear which are not taken into account in the numerical modelling. Figures 8(a) and (b) show the wear track located in the two contact parts after the insertion test. A numerical model with roughness does not sufficiently improve the results (the contact surface under insertion test rapidly become less rough).

4 CONCLUSION

Taking into account the contact zone roughness in numerical modelling led to good contact resistance numerical results in the case of low indentation forces. The roughness influence became negligible in the case of high forces or in the case of the insertion test since the contact surface became very smooth (crushed asperities). In the case of high forces, the spots (due to wear) led to an increase in the contact resistance.

On the other hand, for all materials, the contact resistance in the case of the insertion test was lower than the contact resistance in the case of the indentation test.

It can be concluded that the material which presents the best compromise between the mechanical and electrical aspects is the K80 alloy; even under high forces, this material has the lowest resistance value (Figs 6 and 7) and this presents a low level of permanent deformation in the contact zone. Indeed, Fig. 6 shows that the copper alloys Cub1 and K09 also led to a low electrical contact resistance for high forces, but these two materials have a plastic deformation rate higher than that obtained for the K80 alloy; K80 copper alloy presented a yield stress (322 MPa) higher than that of Cub1 alloy (200 MPa) and K09 alloy (200 MPa) (Table 1).

ACKNOWLEDGEMENTS

The authors express their gratitude to Wieland-Werke AG (Ulm, Germany) for technical assistance

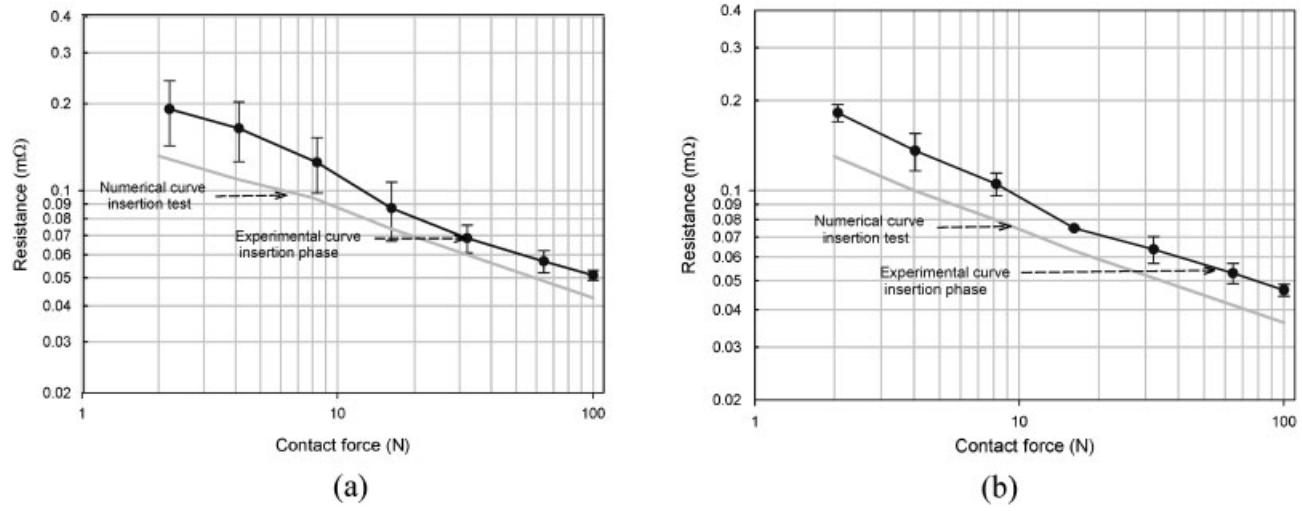

Fig. 13 Contact resistance for the insertion test for (a) Cub1 copper alloy and (b) K09 copper alloy ($R = 3$ mm and $e = 0.8$ mm)

and for material support. This work was supported by the French project EPO-Auto+.

REFERENCES

1 **Ossart, F., Noël, S., Alamarguy, D., Correia, S.,** and **Gendre, P.** Electro-mechanical modelling of multilayer contacts in electrical connectors. In Proceedings of the 53rd IEEE Holm Conference on *Electrical contacts*, Pittsburgh, Pennsylvania, USA, 2007, pp. 1–8 (IEEE, New York).

2 **Queffelec, J. L., Benjemaa, N., Travers, D.,** and **Pethieu, G.** Materials and contact shape studies for automobile connector development. In Proceedings of the 36th IEEE Holm Conference on *Electrical contacts*, Montreal, Canada, 1990, pp. 225–231 (IEEE, New York).

3 **Monnier, A., Froidurot, B., Jarrige, C., Meyer, R.,** and **Testé, P.** A mechanical, electrical, thermal coupled-field. Simulation of a sphere-plane electrical contact. In Proceedings of the 51st IEEE Holm Conference on *Electrical contacts*, Chicago, Illinois, USA, 2005, pp. 224–231 (IEEE, New York).

4 **Zauter, R.** and **Kudashov, D. V.** Precipitation hardened high copper alloys for connector pins made of wire. In Proceedings of the 23rd International Conference on *Electrical contacts (ICEC2006)*, Sendai, Japan, 2006, pp. 257–261 (Institute of Electronics, Information and Communication Engineers, Tokyo).

5 ANSYS, 2005 available from http://www.ansys.com.

6 **Hernot, X., Senouci, A., El Manfalouti, A.,** and **Ben Jemaa, N.** Contact resistance law for elasto-plastic domains in the force range 1 mN–10N. In Proceedings of the International Session on *Electromechanical devices* (*IS-EMD 2002*), vol. 102, no. 452, 2002, pp. 9–13 (Institute of Electronics, Information and Communication Engineers, Tokyo).

7 **Holm, R.** *Electric contacts: theory and applications,* 4th edition, 1999 (Springer-Verlag, Berlin).

8 **Slade, P. G.** *Electrical contacts: principles and applications*, 1999 (Marcel Dekker, New York).

9 **Tangena, A. G.** The correlation between mechanical stresses and wear in layered system. *Wear*, 1988, **121**, 27–35.

10 **El Abdi, R., Benjemaa, N.,** and **Beloufa, M. A.** Numerical and experimental studies of automotive connector behaviour. In Proceedings of the 18th IASTED International Conference on *Modelling and simulation*, Montreal, Canada, 2007, pp. 209–214 (ACTA Press, Anaheim, California).

APPENDIX

Notation

e	sample thickness
E	Young's modulus
F_c	contact force
F_i	indentation force
n	power for the resistance law
P_a	average roughness deviation
P_q	standard roughness deviation
R	sphere radius
R_c	contact resistance
U_x	displacement along the x axis
U_y	displacement along the y axis
ρ	resistivity of the material